several van der Waals contacts (<3.5 Å) with hydrophobic residues of adjacent β and α apoproteins and with both B850 and B800 Bchl *a* molecules. It finishes with its terminal dimethyl groups in contact with His 31 of the adjacent α-apoprotein. It is this residue that is bound to the central Mg of a B850 Bchl *a*. The arrangement of the pigments in the asymmetric unit is shown in Fig. 5.

Energy transfer mechanism

When a Bchl molecule is excited by light, its first excited singlet state lasts for a few nanoseconds[1]. The light-harvesting system must be able to transfer the absorbed energy to the reaction centre in a shorter time than this. Some of the important features that allow this to take place are revealed by the structure reported here.

Previous biophysical studies (reviewed in ref. 1) have shown that energy transfer within the LH2 complex can occur from the B800 to the B850 BChl *a* molecules in 0.7 ps. Once the energy reaches the B850 molecules, it is rapidly transferred among them. This is seen as an ultrafast depolarization of the excited state on the 200–300 fs timescale. Energy transfer from LH2 to LH1 occurs in the 5–20 ps time range, but with LH2 alone the decay of the 850 nm excited singlet state takes 1.1 ns.

The ring of B850 Bchl *a* molecules acts rather like a 'storage ring', with the excited state rapidly delocalized over a large area. The delocalization is facilitated by a highly hydrophobic environment which reduces the dielectric constant, allowing coupling over large distances. The energy is then available for transfer from any part of the ring to any neighbouring LH1 complex. It is clear from electron microscopy imaging of the LH1 complex[13], and from a comparison of the primary structures[3] of the LH2 and LH1 complexes, that the structure of the LH1 complex is similar to that of LH2 (with a larger ring). With such a ring structure, there is no requirement for the LH1 complex to have a special orientation to receive energy from the LH2 ring. Furthermore, because the B875 Bchl *a* molecules in LH1 are liganded to homologous histidine residues, as in LH2, it is likely that the B850 and B875 bacteriochlorophyll rings will be at the same point in the membrane. The overall effect will be to allow energy transfer from any LH2 to any LH1 complex that is within range, without regard to the orientation of either complex. This reduction in the dimensionality of the process will lead to a further kinetic gain.

Previous studies have shown that the carotenoid in this LH2 complex acts as an efficient accessory light-harvesting pigment (>50%)[7]. The excited singlet lifetime of carotenoids is usually less than 10 ps[8]. Therefore, if energy transfer is to compete successfully with these rapid de-excitation processes, the carotenoid must be located very close to the acceptor bacteriochlorophylls[8], as seen in the structure. □

Received 29 December 1994; accepted 13 February 1995.

1. van Grondelle, R., Dekker, J. P., Gillbro, T. & Sundstrom, V. *Biochim. biophys. Acta* **1187,** 1–65 (1994).
2. Hawthornthwaite, A. M. & Cogdell, R. J. in *The Chlorophylls* (ed. Scheer, H.) 493–528 (CRC, Boca Raton, 1993).
3. Zuber, H. & Brunisholz, R. A. in *The Chlorophylls* (ed. Scheer, H.) 627–704 (CRC, Boca Raton, 1993).
4. Gardiner, A. T., Cogdell, R. J. & Takaichi, S. *Photosyn. Res.* **38,** 159–168 (1993).
5. Cogdell, R. J. & Scheer, H. *Photochem. Photobiol.* **42,** 669–689 (1985).
6. Robert, B. & Lutz, M. *Biochim. biophys. Acta* **807,** 10–23 (1985).
7. Angerhofer, A., Cogdell, R. J. & Hipkins, M. F. *Biochim. biophys. Acta* **848,** 333–341 (1986).
8. Frank, H. A. & Cogdell, R. J. in *Carotenoids in Photosynthesis* (eds Young, A. & Britton, G.) 252–326 (Chapman & Hall, London, 1993).
9. Papiz, M. Z. *et al. J. molec. Biol.* **209,** 833–835 (1989).
10. Kuhlbrandt, W., Wang, D. N. & Fujiyoshi, Y. *Nature* **367,** 614–621 (1994).
11. Olsen, J. D. & Hunter, C. N. *Photochem. Photobiol.* **60,** 521–535 (1994).
12. Martinez, S. E., Huang, D., Szczepaniak, A., Cramer, W. A. & Smith, J. L. *Structure* **2,** 95–105 (1994).
13. Karrasch, S., Bullough, P. A. & Ghosh, R. *EMBO. J.* **14,** 631–638 (1995).
14. Leslie, A. G. W. in *Joint CCP4 and ESF-EACMB Newsletter on Protein Crystallography* No. 26 (Daresbury Laboratory, Warrington, 1992).
15. Sheldrick, G. M. *Acta crystallogr.* A**46,** 467–473 (1990).
16. Zhang, K. Y. J. & Main, P. *Acta crystallogr.* A**46,** 377–381 (1990).
17. Cowtan, K. D. & Main, P. *Acta crystallogr.* D**49,** 148–157 (1993).
18. Collaborative Computational Project, No. 4 *Acta crystallogr.* D**50,** 760–766 (1994).
19. Wang, B. C. *Meth. Enzym.* **115,** 90–112 (1985).
20. Matthews, B. W. *J. molec. Biol.* **33,** 491–497 (1968).
21. Brunger, A. T. *Nature* **335,** 472–475 (1992).
22. Jones, T. A., Zou, J. Y., Cowan, S. W. & Kjeldgaard, M. *Acta crystallogr.* A**47,** 110–119 (1991).
23. Brunger, A. T. *XPLOR Version* 3.1 *Manual* (Yale Univ., USA, 1993).
24. Hendrickson, W. A. *Meth. Enzym.* **115,** 252–270 (1985).

ACKNOWLEDGEMENTS. We thank P. Emsley for help with general computations. Some diffraction data were collected at the EMBL synchrotron source, Hamburg, and the assistance of K. S. Wilson and Z. Dauter is gratefully acknowledged. This work has been supported by the BBSRC Membrane Initiative and the E.C. R.J.C. dedicates this paper to H. Zuber and J. P. Thornber, fathers of this area of research.

Observational confirmation of a circumsolar dust ring by the COBE satellite

W. T. Reach*, B. A. Franz†, J. L. Weiland‡, M. G. Hauser§, T. N. Kelsall§, E. L. Wright‖, G. Rawley†, S. W. Stemwedel† & W. J. Spiesman¶

* Universities Space Research Association, NASA Goddard Space Flight Center, Code 685, Greenbelt, Maryland 20771, USA
† Applied Research Corporation, ‡ General Sciences Corporation, NASA GSFC, Code 685.3, Greenbelt, Maryland 20771, USA
§ NASA GSFC, Code 680, Greenbelt, Maryland 20771, USA
‖ UCLA Astronomy Department, Los Angeles, California 90024, USA
¶ McDonald Observatory, University of Texas, Austin, Texas 78712, USA

ASTEROID collisions are an important source of the dust particles in the zodiacal cloud[1–3]. These particles spiral in towards the Sun under the influence of drag forces[4–6] and, in passing through the inner Solar System, are subject to gravitational perturbations by the planets, which may trap them (at least temporarily) in orbital resonances[7–10]. Recently, numerical simulations have shown that resonances with the Earth are particularly effective at trapping asteroidal dust, leading to the suggestion that the Earth may be embedded in a circumsolar ring of dust[11]. The azimuthal structure of this ring was predicted to be asymmetric, with the region trailing the Earth being substantially more dense than that in the leading direction[11]. This prediction is in both qualitative and quantitative agreement with the asymmetry in zodiacal light observed by the Infrared Astronomical Satellite (IRAS)[11,12], but the IRAS data alone are equivocal because of calibration uncertainties and sparse coverage of elongation angle[12]. Here we report observations by the Diffuse Infrared Background Experiment[13] (DIRBE) on the Cosmic Background Explorer satellite (COBE)[14], which confirm both the existence of this ring and the predictions of its near-Earth structure.

DIRBE mapped the entire sky with a 0.7° beam in ten wavebands (1.25, 2.2, 3.5, 4.9, 12, 25, 60, 100, 140 and 240 μm). The DIRBE instrument measured the sky brightness relative to an internal zero-brightness reference source, thus eliminating the calibration uncertainty of IRAS. The viewing geometry for DIRBE is illustrated in Fig. 1. The COBE satellite orbits the Earth along the terminator, and it spins at 0.8 r.p.m. about an axis nearly perpendicular to the Earth–Sun line. The DIRBE field of view is offset 30° from the spin axis. The combination

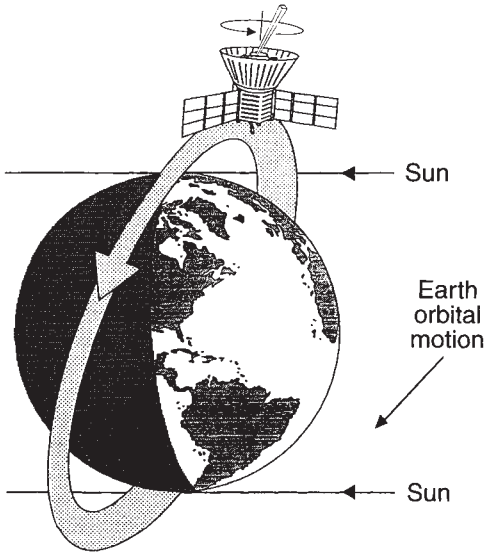

FIG. 1 The viewing geometry for DIRBE. The COBE satellite orbit is close to the terminator, and the spin axis is kept nearly perpendicular to the Sun. COBE is shown at one point in its orbit, with the DIRBE field of view extending outwards at an angle of 30° from the spin axis.

of orbital motion and spacecraft rotation causes the DIRBE field of view to trace a helical path on the sky within two viewing swaths, each 60° wide. These swaths, which correspond to observations with the satellite closer to the apex and antapex of the Earth's orbit about the Sun, are called the 'leading' and 'trailing' swaths. Using one week of data, the two viewing swaths are well sampled. An example of a weekly map in the 12-μm waveband is shown in Fig. 2*a*. The position of the Sun has been rotated to the centre of the map for convenience, and lines of sight trailing the Earth, which have ecliptic longitudes greater than that of the Sun, appear left of centre.

First, we attempted to confirm the brightness asymmetry observed by IRAS, such that the zodiacal light was brighter when viewed along lines of sight trailing the Earth than when viewed leading the Earth. The peak zodiacal light brightness occurs at an ecliptic latitude that varies with time of year, and there is mid-infrared emission from Galactic dust, so we took care to separate these effects. We extracted DIRBE data in scans from the North Ecliptic Pole to the South Ecliptic Pole and back to the North again, in weekly intervals throughout the mission. Each scan was fitted with an empirical function that accurately matches the angular variation of the zodiacal light[13]. Portions of the scans within 20° of the Galactic plane were excluded, and a cosecant model of the emission from the Galaxy was fitted to the scans simultaneously with the empirical zodiacal light function. The polar brightnesses of the leading and trailing portions of the scan were forced to agree, as indeed they must. This removes one of the difficulties—namely scan-to-scan calibration errors—that was faced in measuring the trailing–leading asymmetry from the IRAS data[12]. The peak zodiacal light brightness is shown as a function of time in Fig. 3. The brightness trailing the Earth was in fact greater than that leading the Earth throughout the mission by ~2–3%, confirming observations by IRAS[11,12]. The fact that the trailing scans are always brighter indicates that the brightness asymmetry is corotating with the Earth. A fixed longitudinal variation in the dust density would

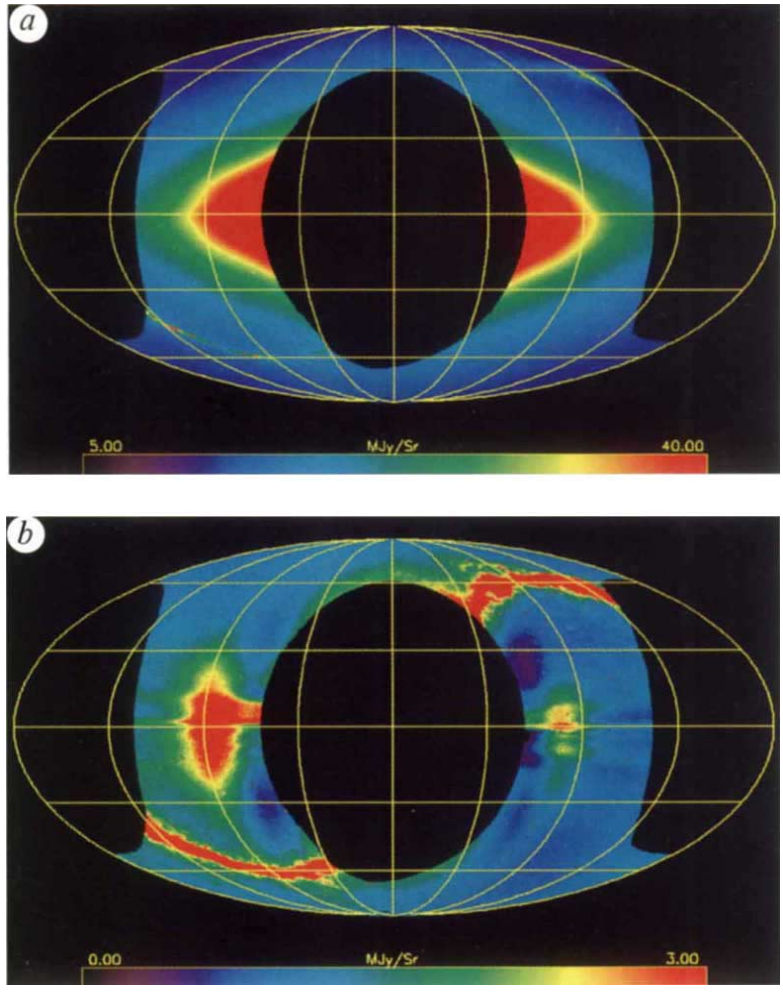

FIG. 2 *a*, Map of the sky brightness observed by DIRBE in the 12-μm waveband during the one-week period beginning on 2 July 1990. The map is projected into ecliptic coordinates with the Sun in the centre and the North and South ecliptic poles at the top and bottom, respectively. The black region in the centre is the Sun-avoidance region. The two viewing swaths to the left and right of the Sun-avoidance region cover lines of sight trailing and leading the Earth, respectively. *b*, As *a*, but after the subtraction of a three-dimensional model for the interplanetary dust cloud. Note that the bulk of the sky brightness was subtracted, and the colour table was adjusted to reveal the much fainter residual brightness. The bright S-shaped ridge of emission from lower left to upper right is the Milky Way. The regions of enhanced brightness 90° from the Sun are the signature of the circumsolar dust ring.

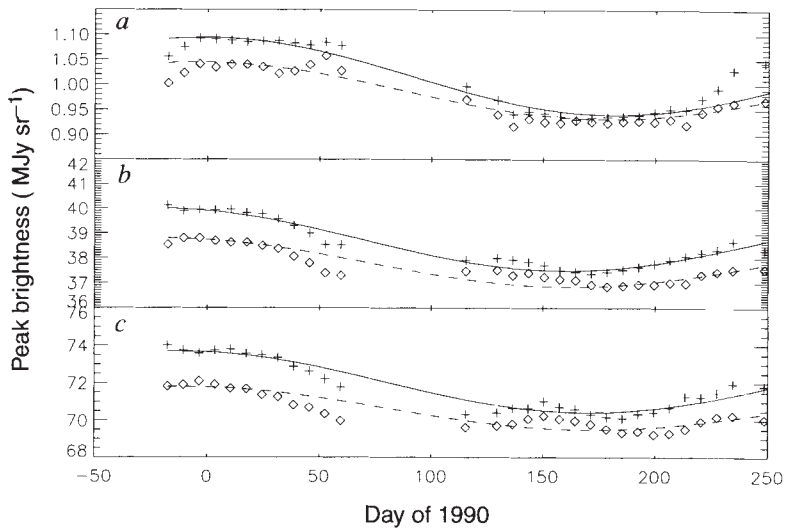

FIG. 3 The peak brightness of the zodiacal light observed at a solar elongation of 90° is shown as a function of time throughout the DIRBE mission at three wavelengths: *a*, 4.9 μm; *b*, 12 μm; *c*, 25 μm. Gaps in the plotted data are times when the Galaxy could not be easily separated from the zodiacal light. The brightness trailing the Earth (+symbols) was brighter than that leading the Earth (◇) throughout the mission, demonstrating that the region of enhanced brightness followed the Earth. The curves drawn through the data are sinusoidal fits, with a period of one year, for the trailing (solid curve) and leading (dashed) brightness.

cause the trailing scans to be brighter for six months, then the leading scans brighter for the other six months. The trailing–leading brightness difference is apparently not constant, being largest when the Earth is near perihelion and smallest when the Earth is near aphelion. The temporal variation of the trailing–leading brightness difference may be due to the motion of the Earth with respect to the dust ring—an effect that is predicted based on the numerical simulations[11].

Using the trailing–leading brightness asymmetry, we measured the temperature and albedo of the grains in the dust ring. In January 1990, the trailing–leading brightness differences were 0.05 ± 0.01, 1.1 ± 0.2 and 1.7 ± 0.1 MJy sr^{-1} (10^{-17} erg cm^{-2} s^{-1} Hz^{-1} sr^{-1}) at wavelengths of 4.9, 12 and 25 μm, respectively. The colour temperature of the brightness asymmetry is 290 ± 15 K, similar to the temperature of the zodiacal light[16] and comparable to expectations for particles, 10–100 μm in radius, composed of at least moderately absorbing material[15]. The trailing–leading asymmetry is marginally detected at 1.25 μm, with a brightness of 0.013 ± 0.003 MJy sr^{-1} indicating a geometric albedo of 0.3 ± 0.1, consistent with that of the other cloud particles[16].

Using the weekly sky maps created by DIRBE, we were able to image for the first time the structure responsible for the trailing–leading brightness asymmetry. To remove the emission from relatively smoothly distributed dust, we have fitted a model of the sky brightness based on integrating along each line of sight a parametrized model for the density and temperature of interplanetary dust. The cloud was assumed to be cylindrically symmetric as well as reflection-symmetric about a midplane, with a density of the form[17–19]

$$n(r, z) = n_0 r_{xy}^{-\alpha} \exp(-\beta |z/r_{xy}|^{\gamma}) \quad (1)$$

where r_{xy} is the distance from the cloud centre in the midplane, and z is the vertical distance from the midplane. The location of the cloud centre with respect to the Sun and the tilt and ascending node of the midplane were fitted. The grain temperatures were assumed to vary as $T = T_0 r^{-\delta}$, with $T_0 = 286$ K determined from the 4.9–25 μm colour. Scattering in the near-infrared (1.2, 2.2 and 3.5 μm) was modelled using a scattering phase function consisting of three Henyey–Greenstein functions[20]. The albedo in each near-infrared band and the emissivity in each of the thermal emission bands (3.5–240 μm) were free parameters. In addition to the smooth cloud model, the band-pair that appears near ±10° was fitted using a parametrized form based on the 'migrating' band model[6].

The smooth cloud model was fitted to lines of sight observed leading the Earth only, because the trailing lines of sight are predicted to be more affected by the dust ring. The parameters $\alpha = 1.39 \pm 0.03$, $\beta = 3.26 \pm 0.04$, $\gamma = 1.02 \pm 0.01$ and $\delta = 0.42 \pm 0.01$ were optimized, and the density at 1 AU is $n_0\sigma = (7.6 \pm 0.1) \times 10^{-21}$ cm^{-1}—some 65% larger than that inferred from *in situ* observations of meteoroids[21]. The residual map, after the smooth cloud model was subtracted from the map in Fig. 2*a*, is shown in Fig. 2*b*. This Figure should be compared with the simulated all-sky view given on the cover of the 30 June 1994 issue of *Nature*[11]. Two regions of enhanced brightness leading and trailing the Earth are evident, with the latter region substantially brighter. The region of enhanced brightness trailing the Earth is centred ~90° from the Sun, and that leading the Earth is centred ~80° from the Sun. The full-width at half-maximum brightness of the trailing region is 30° in latitude and 15° in longitude. These observations are in remarkable agreement with the predictions for small particles in orbital resonance with the Earth[11]. Based on the excess brightness of the trailing region and its predicted size along the line of sight, its peak volumetric cross-section (density times cross-section) is $\langle n\sigma \rangle \approx 3 \times 10^{-21}$ cm^{-1}, nearly half that of the smooth cloud model at 1 AU. □

Received 18 November 1994; accepted 21 February 1995.

1. Low, F. J. *et al. Astrophys. J.* **278,** L19–L22 (1984).
2. Dermott, S. F., Nicholson, P. D., Burns, J. A. & Houck, J. R. *Nature* **312,** 505–509 (1984).
3. Sykes, M. V. *Icarus* **84,** 267–289 (1990).
4. Wyatt, S. P. & Whipple, F. L. *Astrophys. J.* **111,** 134–141 (1950).
5. Burns, J. A., Lamy, P. L. & Soter, S. *Icarus* **40,** 1–48 (1979).
6. Reach, W. T. *Astrophys. J.* **392,** 289–299 (1992).
7. Jackson, A. A. & Zook, H. A. *Nature* **337,** 629–631 (1989).
8. Jackson, A. A. & Zook, H. A. *Icarus* **97,** 70–84 (1992).
9. Sicardy, B., Beaugé, C., Ferraz-Mello, S., Lazzaro, D. & Roques, F. *Celestial Mech. dynamical Astr.* **57,** 373–390 (1993).
10. Weidenschilling, S. J. & Jackson, A. A. *Icarus* **104,** 244–254 (1993).
11. Dermott, S. F., Jayraraman, S., Xu, Y. L., Gustafson, B. Å. S. & Liou, J. C. *Nature* **369,** 719–723 (1994).
12. Reach, W. T. *Astrophys. J.* **369,** 529–543 (1991).
13. Hauser, M. G. in *Back to the Galaxy* (eds Holt, S. & Verter, F.) 201–205 (Am. Inst. Phys, New York, 1993).
14. Boggess, N. W. *et al. Astrophys. J.* **397,** 420–429 (1992).
15. Reach, W. T. *Astrophys. J.* **335,** 468–485 (1988).
16. Spiesman, W. J. *et al. Astrophys.* (in the press).
17. Leinert, C. *Space Sci. Rev.* **18,** 281–339 (1975).
18. Giese, R. H., Kneissel, B. & Rittich, U. *Icarus* **68,** 395–411 (1986).
19. Good, J. C., Gautier, T. N. & Hauser, M. G. *Adv. Space Res.* **6,** 84–86 (1986).
20. Hong, S. S. *Astr. Astrophys.* **146,** 67–75 (1985).
21. Grün, E., Zook, H. A., Fechtig, H. & Giese, R. H. *Icarus* **62,** 244–272 (1985).

ACKNOWLEDGEMENTS. W. T. R. thanks S. Jayraraman and S. F. Dermott for discussions, and R. F. Silverberg, J. C. Mather and G. A. Toller for reviews. We thank R. G. Arendt for help with Fig. 1. This work was supported by NASA's COBE project. The National Aeronautics and Space Administration/Goddard Space Flight Center (NASA/GSFC) is responsible for the design, development and operation of COBE. Scientific guidance is provided by the COBE Science Working Group. GSFC is also responsible for the development of the analysis software and for the production of the mission data sets.